Electronic structure and cohesive energy of silylmethyl fullerene and methanoindene fullerene solids

著者（英）	Sho Furutani, Yutaka Matsuo, Susumu OKADA
journal or publication title	Japanese journal of applied physics
volume	57
number	8
page range	085102
year	2018-07
権利	(C) 2018 The Japan Society of Applied Physics
URL	http://hdl.handle.net/2241/00154187

doi: 10.7567/JJAP.57.085102

Electronic structure and cohesive energy of silyl methyl fullerene and methano indene fullerene solids

Sho Furutani[1], Yutaka Matsuo[2,3], and Susumu Okada[1]*

[1]*Graduate School of Pure and Applied Sciences, University of Tsukuba, Tsukuba, Ibaraki 305-8571, Japan*
[2]*Department of Mechanical Engineering, The University of Tokyo, Bunkyo, Tokyo 113-8656, Japan*
[3]*Hefei National Laboratory for Physical Sciences at the Microscale and Department of Chemistry, School of Chemistry and Materials Sciences, University of Science and Technology of China, Hefei, Anhui 230026, China*

Using the density functional theory, we studied the energetics and electronic structures of chemically decorated fullerene solids, monoclinic phases of silyl methyl fullerene (SIMEF) and methano indene fullerene (MIF), under the experimentally determined lattice parameters. Cohesive energies of these solids are 1.83 and 1.07 eV for SIMEF and MIF, respectively, despite the large intermolecular spacing owing to the functional groups. The SIMEF and MIF solids are semiconductors with a moderate band gap of about 1.2 eV with narrow dispersion band near the band gap. We also elucidated that these solids exhibit a strong anisotropic band dispersion relation near the gap, because of their large asymmetric molecular shape. The calculated electron effective masses range from 1.37m_e to 7.91m_e for the SIMEF solid and from 0.57m_e to 4.23m_e for the MIF solid.

1. Introduction

Ever since the discovery[1)] and macroscopic production[2)] of fullerenes, fullerenes have been keeping a premier position in nanoscale sciences and technologies, because of the diversity of their geometry and corresponding electronic properties.[3–5)] Because of the hollow-cage structures of fullerenes, electronic structures near the Fermi level of fullerenes can be characterized as a spherical harmonic Y_{lm}, where the electronic states associated with π electrons tend to bunch up or become degenerate with each other, reflecting their approximately spherical distribution in the fullerene cage.[6)] Thus, the π electron states are often naively regarded as an electron system confined to the spherical shell with a nanometer-scale diameter.[7)] In addition, fullerenes commonly possess a deep lowest unoccupied state, compared with other carbon nanomaterials and hydrocarbon molecules,[8,9)] owing to the twelve pentagonal rings embedded in their cages.[6)]

*E-mail: sokada@comas.frsc.tsukuba.ac.jp

Therefore, fullerenes can act as electron acceptors for electrochemical and photovoltaic applications. On the other hand, the detailed electronic structure of fullerenes depends not only on the fullerene cage size but also on the local atomic arrangement, owing to the strong correlation between the geometry and the electronic properties as cases of the polycyclic aromatic hydrocarbons. For example, the electronic structures of the 24 isomers of C_{84} are completely different from each other, depending on variations in their covalent network topology, even though each isomer has the same cage size.[10,11] Furthermore, the moderate chemical reactivity of fullerenes allows us to design and synthesize further derivatives by attaching atoms[12,13] or functional groups[14–19] onto the cage. In this case, the electronic structure of these fullerene derivatives is different from that of pristine fullerenes because of the modification of the π electron network.[20–22]

Silyl methyl fullerene (SIMEF)[23] and methano indene fullerene (MIF)[24] are representative fullerene derivatives that act as electron acceptors in blends with appropriate donor molecules in organic thin film photovoltaic devices. Using these chemically decorated fullerenes, photovoltaic devices can show large open voltages owing to the deep lowest unoccupied state of the fullerenes[25–30] and a remarkable power conversion efficiency of up to about 10 %.[31] In the devices, molecular conformations of SIMEF and MIF in their condensed structure and with respect to the donor domains are important in realizing the high electron mobility in acceptor domains and the effective carrier dissociation at the donor-acceptor interfaces, respectively, which are key issues in further improving the power conversion efficiency of the devices. For the interface, we demonstrated that the molecular orientation with respect to the donor domain is important in realizing the field concentration at the interface, causing the efficient carrier dissociation at the interfaces.[22] On the other hand, the electronic structure of bulk condensed phases of SIMEF and MIF is still unclear. Thus, in this work, we aim to clarify the electronic properties of bulk condensed phases of SIMEF and MIF using the density functional theory (DFT). Our calculations indicate that the electronic band structure of SIMEF and MIF solids is anisotropic arising from their asymmetric molecular shape due to functional groups.

2. Calculation methods and structural models

All theoretical calculations were conducted using the DFT[32,33] implemented in the STATE package.[34] To express the exchange correlation potential among the interacting electrons, the local density approximation (LDA) was applied with the Perdew-Wang

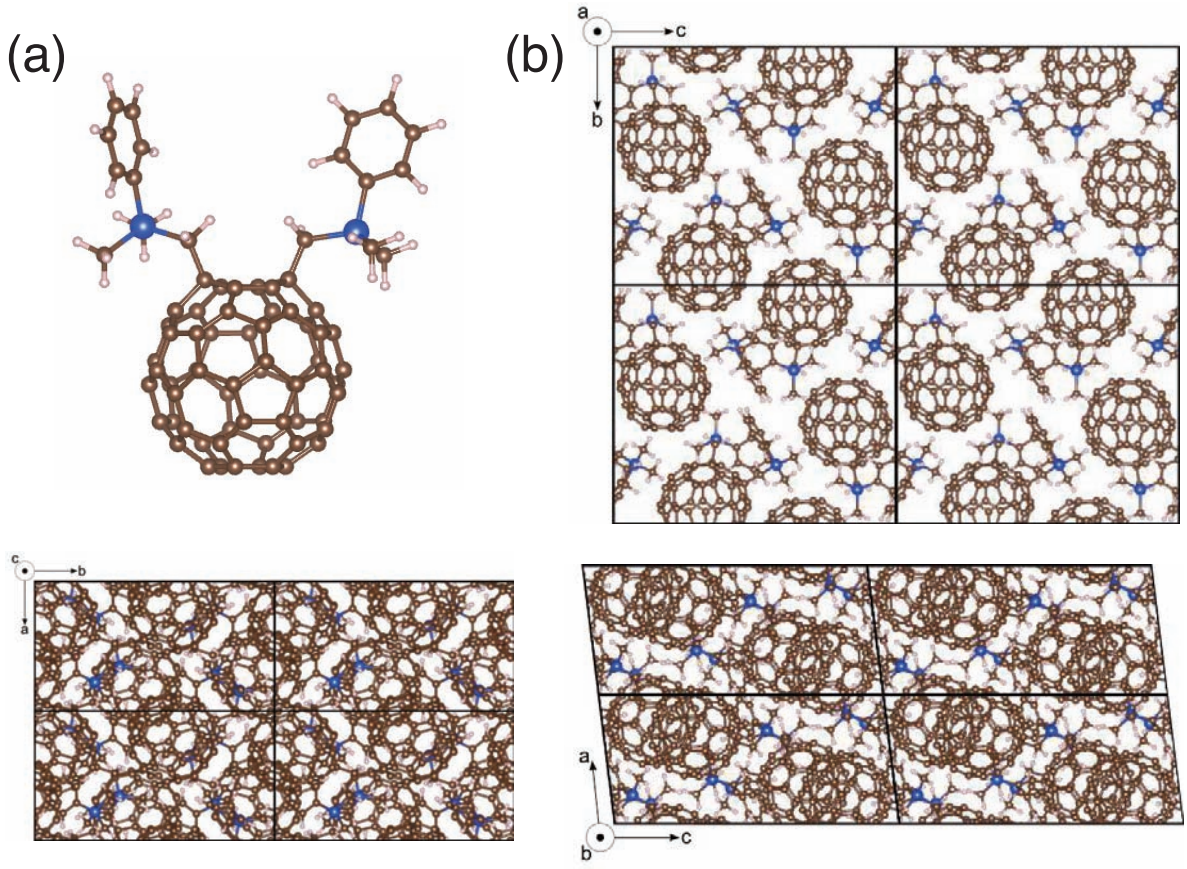

Fig. 1. Optimized geometries of SIMEF in (a) an isolated form and (b) a packed structure with a monoclinic phase under the experimentally determined lattice constant. Brown, blue, and white balls denote C, Si, and H atoms, respectively. In each figure, quadrangles indicate the unit cell.

functional form fitted to the quantum Monte Carlo results for a homogeneous electron gas,[35,36] because LDA can qualitatively describe the weak interactions between graphitic sp^2 C materials. We used an ultrasoft pseudopotential to describe the interactions between the valence electrons and the ions generated by the Vanderbilt scheme.[37] The valence wave functions and deficit charge density were expanded by a plane-wave basis set with cutoff energies of 25 and 225 Ry, respectively. Brillouin zone integration was carrier out using equidistant 4×4×4-$\boldsymbol{k}$ meshes that give sufficient convergence in the geometric and electronic structures of fullerene related materials.[38] Structural optimization was performed for both internal atomic coordinates under the experimentally determined lattice constant until the remaining force acting on each atom was less than 5 mRy/Å.

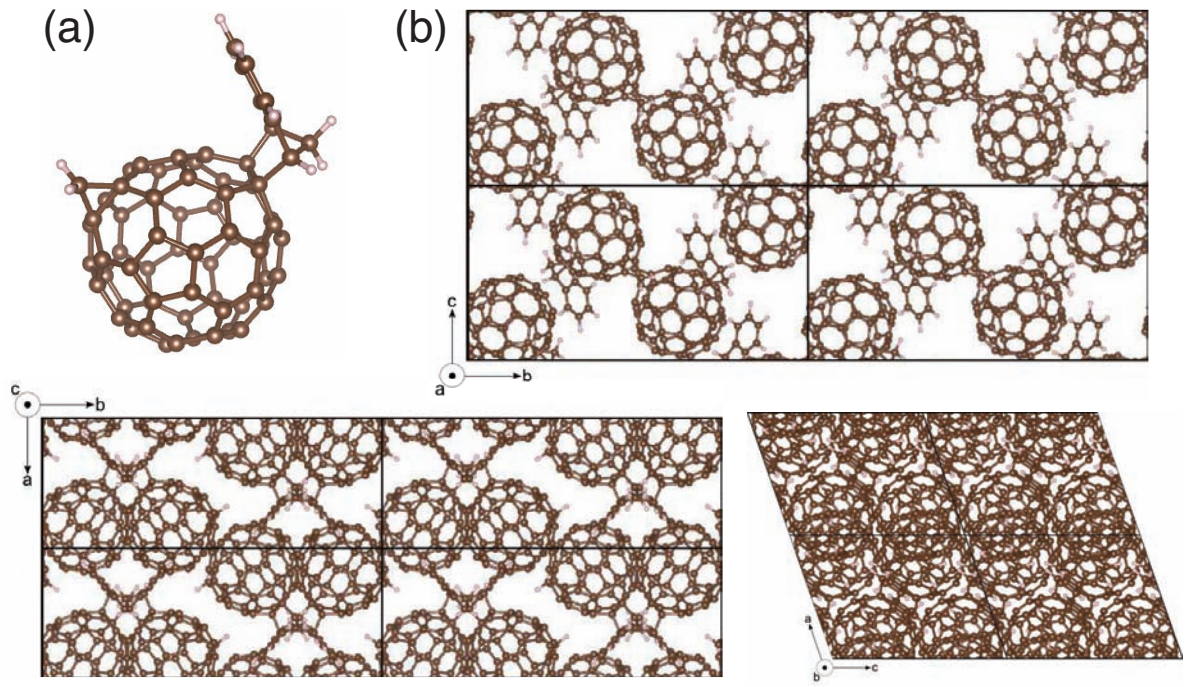

Fig. 2. Optimized geometries of MIF in (a) an isolated form and (b) a packed structure with a monoclinic phase under the experimentally determined lattice constant. Brown and white balls denote C and H atoms, respectively. In each figure, quadrangles indicate the unit cell.

3. Results and discussion

Figure 1 shows the optimized structure of an isolated SIMEF molecule and a SIMEF solid under the lattice parameters determined by X-ray diffraction experiment.[39,40] The SIMEF solid has a monoclinic lattice structure with the cell parameters a=10.36 Å, b=19.02 Å, c=22.67 Å, α=90°, β=97.13°, and γ=90°. Figure 2 shows the optimized structure of an isolated MIF molecule and a MIF solid in the monoclinic structure under the lattice parameters a=10.69 Å, b=26.52 Å, c=14.40 Å, α=90°, β=109.04°, and γ=90° determined by X-ray diffraction experiment.[41,42] Because of the asymmetric shape of SIMEF and MIF, the monoclinic unit cell contains 4 molecules to form approximately closed packed structure with the staggered intermolecular arrangement. Under the experimentally determined lattice parameters, the cohesive energies of SIMEF and MIF are 1.83 and 1.07 eV per molecule, respectively. The calculated cohesive energy is comparable to that of the pristine C_{60} in its condensed phase, although SIMEF and MIF exhibit large intermolecular spacings. The large cohesive energy of chemically decorated C_{60} is ascribed to the silyl methyl and methano indene functional groups attached to SIMEF and MIF, respectively, which cause polarization on chemically dec-

orated fullerenes. Thus, in addition to the weak intermolecular interaction, the polar and CH-π interactions between functional groups and C_{60} moieties cause the large cohesive energy in their condensed phases, even though they have large intermolecular spacings owing to the steric hindrance of the functional groups.

Figure 3(a) shows the electronic energy band of the SIMEF solid. The solid is an indirect gap semiconductor with a band gap of 1.2 eV around the Γ point. The valence band top is located at the vicinity of the B point along the line connecting between B and Γ points, and the conduction band bottom is located at the Γ point. Because of its large intermolecular spacing, the SIMEF solid exhibits a small dispersion in both the valence and conduction bands, owing to the small π-π overlap between adjacent SIMEFs. The calculated band widths of the highest valence and the lowest conduction bands are 0.1 and 0.2 eV, respectively, which are remarkably narrower than those of the solid C_{60} with a face-centered cubic lattice by about 0.3 eV. Furthermore, the asymmetric shape of the molecule causes a strong anisotropy in both valence and conduction bands. Around the conduction band edge at Γ point, the dispersion along the Γ-Z and the Γ-B direction is narrower than that along the Γ-Y and Γ-A direction. Thus, the effective electron masses at the conduction band bottom also exhibit a remarkable anisotropy: The calculated effective masses at the Γ point are $5.69m_e$, $1.37m_e$, $7.91m_e$, and $3.83m_e$ along the direction to the Z, Y, B, and A points, respectively.

Figure 3(b) shows the squared wave functions of the the highest occupied and the lowest unoccupied states of an isolated SIMEF molecule. The wave functions of the highest and the lowest unoccupied states are distributed on the C_{60} moiety. Therefore, the functional moiety acts as a molecular spacer for the electron states associated with the highest occupied and lowest unoccupied states. Therefore, the functional group causes the large molecular spacing and the small band dispersion near the Fermi level. Around the conduction band edge, the 8 bunched branches are ascribed to the lowest and the second lowest unoccupied states of the SIMEF molecule. In contrast, the isolated four branches in the valence band edge are ascribed to the highest occupied state of the isolated molecule.

Figure 4(a) shows the electronic structure of the MIF solid. The MIF solid is a semiconductor with a direct band gap of 1.27 eV at the Γ point. The large intermolecular spacing arising from the functional groups causes the small band dispersion in both the valence and conduction bands. The bandwidth of the conduction band is wider than that of the valence band by 0.2 eV, as in the SIMEF solid. Furthermore, an asymmetric

shape of the MIF also causes the anisotropic band structure near the gap. In particular, the lowest four branches of the conduction band exhibit remarkable anisotropy. The calculated effective electron masses at the Γ point are $0.57m_e$, $3.48m_e$, $4.23m_e$, and $3.96m_e$ along the direction to the Z, Y, B, and A points, respectively. Thus, the electron mass along the direction along the *c*-axis is the remarkably smaller than that of those along the other directions. This anisotropic electronic structure near the band gap of the MIF solid is also attributed from the wavefunction distribution of the highest occupied and the lowest unoccupied states [Fig. 3(b)]. As in the case of the isolated SIMEF molecule, both the highest occupied and lowest unoccupied states are distributed on the C_{60} moiety, but absent on the functional moiety. Thus, the wavefunction overlap between the adjacent molecules is sensitive to the molecular conformation with regard to the C_{60} moiety in their packed structure.

4. Conclusions

Using the DFT with LDA, we studied the electronic structure of the SIMEF and MIF solids under the experimentally determined lattice parameters. Cohesive energies of these solids are 1.83 and 1.07 eV for SIMEF and MIF, respectively, despite the large intermolecular spacing owing to the functional groups. The SIMEF and MIF solids are semiconductors with a moderate band gap of about 1.2 eV with a narrow dispersion band in their valence and conduction states near the band gap. We also elucidated that the solids exhibit a strong anisotropic band dispersion relation near the gap because of their large asymmetric molecular shape. The calculated electron effective masses range from $1.37m_e$ to $7.91m_e$ for the SIMEF solid and from $0.57m_e$ to $4.23m_e$ for the MIF solid. Thus, it is important to tune the direction of electron transport with respect to the bulk structure for further enhancement of the power conversion efficiency of the photovoltaic devices using these molecules.

Acknowledgements

This work was supported by JST-CREST Grant Numbers JPMJCR1532 and JPMJCR1715 from the Japan Science and Technology Agency, JSPS KAKENHI Grant Numbers JP17H01069 and JP16H06331 from the Japan Society for the Promotion of Science, and the Joint Research Program on Zero-Emission Energy Research, Institute of Advanced Energy, Kyoto University. Part of the calculations was performed on an NEC SX-Ace at the Cybermedia Center at Osaka University and on an SGI ICE

XA/UV at the Institute of Solid State Physics, The University of Tokyo.

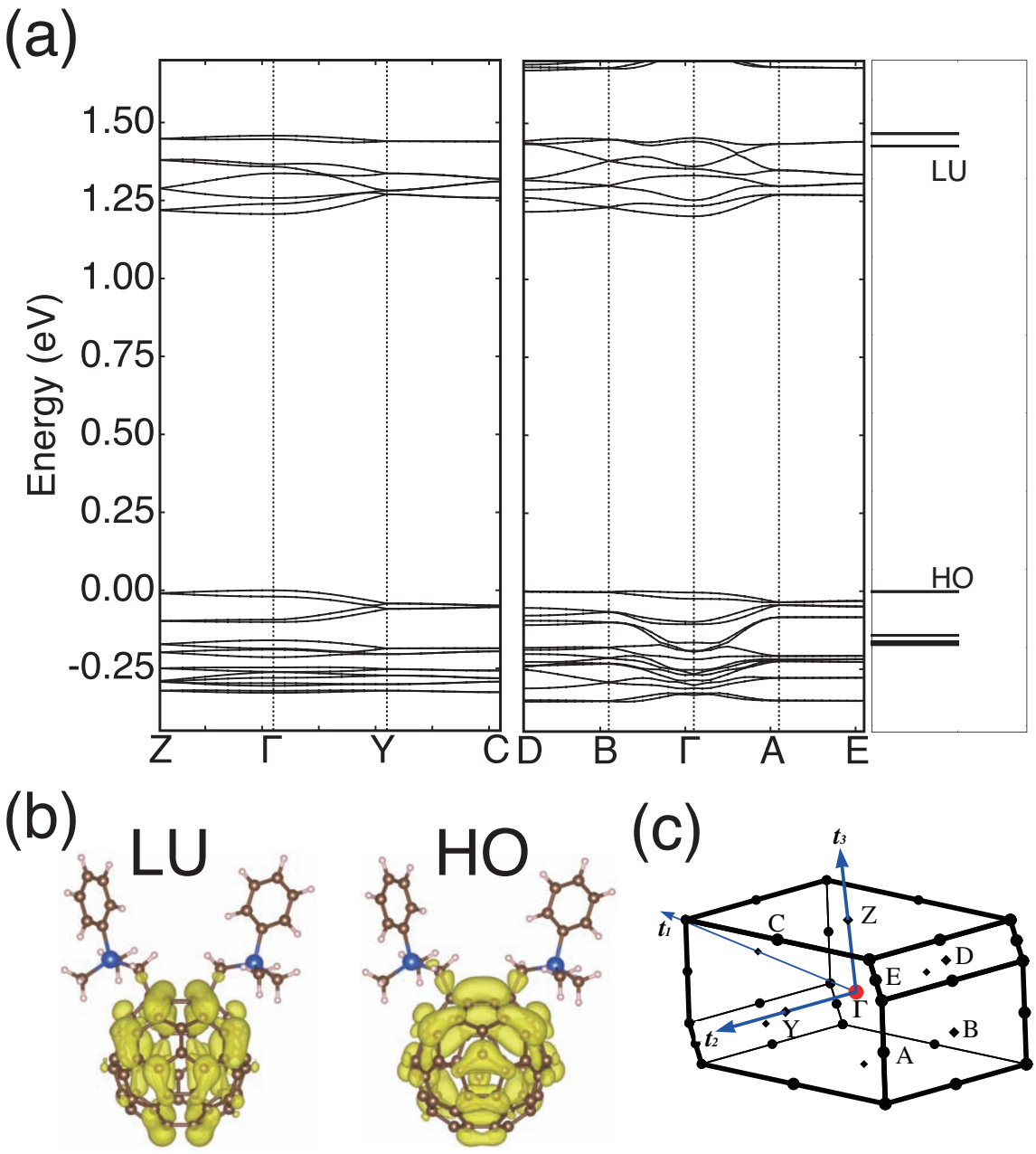

Fig. 3. (a) Electronic energy band and energy level of the SIMEF solid under the experimentally determined lattice parameters and the isolated SIMEF molecule, respectively. The energy is measured from the valence band top. (b) Squared wave functions of the lowest unoccupied (LU) and highest occupied (HO) states of the SIMEF molecule. (c) Brillouin zone and the reciprocal points for calculating the electronic energy band. $\boldsymbol{t}_i$ indicates the primitive reciprocal vector associated with the primitive vector $\boldsymbol{a}_i$.

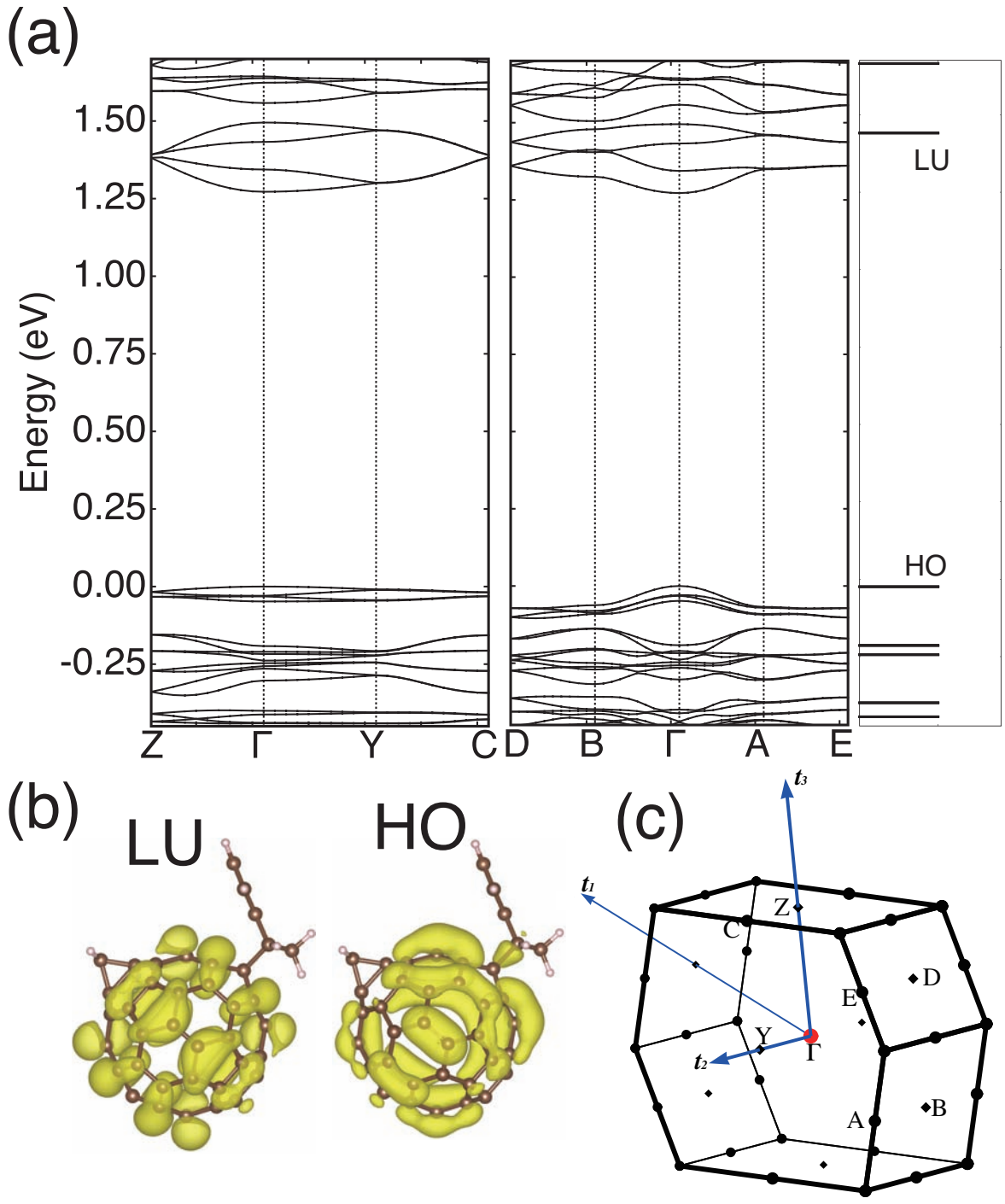

Fig. 4. (a) Electronic energy band and energy level of the MIF solid under the experimental lattice parameters and the isolated MIF molecule, respectively. The energy is measured from the valence band top. (b) The squared wave functions of the lowest unoccupied (LU) and highest occupied (HO) states of the MIF molecule. (c) Brillouin zone and the reciprocal points for calculating the electronic energy band. $\boldsymbol{t}_i$ indicates the primitive reciprocal vector associated with the primitive vector $\boldsymbol{a}_i$.

References

1) H. W. Kroto, J. R. Heath, S. C. O'Brien, R. F. Curl, R. E. Smalley, Nature **318**, 162 (1985).
2) W. Krätschmer, L. D. Lamb, K. Fostiropoulous, D. R. Hoffman, Nature **347**, 354 (1990).
3) M. S. Dresselhaus, G. Dresselhaus, and P. C. Eklund, *Science of Fullerenes and Carbon Nanotubes* (Academic Press, San Diego, CA, 1996)/
4) P. W. Fowler and D. E. Manolopoulos, *An Atlas of Fullerenes*, (Oxford University Press, Oxford, U. K., 1995).
5) D. E. Manolopoulos and P. W. Fowler, J. Chem. Phys. **96**, 7603 (1992).
6) S. Saito, S. Okada, S. -I. Sawada, and N. Hamada, Phys. Rev. Lett. **75**, 685 (1995).
7) J. Sorimachi and S. Okada, Chem. Phys. Lett. **659**, 1 (2016).
8) S. Okada, S. Saito, and A. Oshiyama, Phys. Rev. Lett. **86**, 3835 (2001).
9) Y. A. Saucier, S. Okada, and M. Maruyama, Appl. Phys. Express **10**, 095101 (2017)
10) B. L. Zhang, C. Z. Wang, and K. M. Ho, Chem. Phys. Lett. **193**, 225 (1992).
11) B. L. Zhang, C. Z. Wang, K. M. Ho, C. H. Xu, and C. T. Chan, J. Chem. Phys. **98**, 3095 (1993).
12) F. N. Tebbe, R. L. Harlow, D. B. Chase, D. L. Thorn, G. C. Campbell, J. C. Calabrese, N. Herron, R. J. Young, and E. Wasserman, Science **256**, 822 (1992).
13) J. H. Holloway, E. G. Hope, R. Taylor, G. J. Langley, A. G. Avent, T. J. Dennis, J. P. Hare, H. W. Kroto, and D. R. M. Walton, J. Chem. Soc. Chem. Commun. **12**, 966 (1991).
14) Y. Matsuo and E. Nakamura, Chem. Rev. **108**, 3016 (2008).
15) T. Akasaka, F. Wudl, and S. Nagase, Chemistry of Nanocarbons, Wiley, West Sussex, 2010.
16) M. Sawamura, K. Kawai, Y. Matsuo, K. Kanie, T. Kato, and E. Nakamura, Nature **419**, 702 (2002).
17) Y. Matsuo, A. Muramatsu, R. Hamasaki, N. Mizushita, T. Kato, and E. Nakamura, J. Am. Chem. Soc. **126**, 432 (2004).
18) E. Nakamura, K. Tahara, Y. Matsuo, and M. Sawamura, J. Am. Chem. Soc. **125**, 2834 (2003).
19) Y. Matsuo and E. Nakamura, J. Am. Chem. Soc. **127**, 8457 (2005).

20) S. Okada, R. Arita, Y. Matsuo, E. Nakamura, A. Oshiyama, and H. Aoki, Chem. Phys. Lett. **399**, 157 (2004).

21) H. Nitta, Y. Matsuo, E. Nakamura, and S. Okada, Appl. Phys. Exp. **6**, 045102 (2013).

22) S. Furutani and S. Okada, Chem. Phys. Lett. **678**, 5 (2017).

23) Y. Zhang, Y. Matsuo, C. -Z. Li, H. Tanaka, and E. Nakamura J. Am. Chem. Soc. **133**, 8086 (2011).

24) Y. Matsuo, A. Iwashita, Y. Abe, C. -Z. Li, K. Matsuo, M. Hashiguchi and E. Nakamura, J. Am. Chem. Soc. **130**, 5429 (2008).

25) M. C. Scharber, D. Muhlbacher, M. Koppe, P. Denk, C. Waldauf, A. J. Heeger, and C. J. Brabec, Adv. Mater. **18**, 789 (2006).

26) F. B. Kooistra, J. Knol, F. Kastenberg, L. M. Popescu, W. J. H. Verhees, J. M. Kroon, and J. C. Hummelen, Org. Lett. **9**, 551 (2007).

27) Y. Matsuo, Y. Sato, T. Niinomi, I. Soga, H. Tanaka, and E. Nakamura, J. Am. Chem. Soc. **131**, 44 (2009).

28) Y. Matsuo, Chem. Lett. **41**, 754 (2012).

29) A. Sanchez-Diaz, M. Izquierdo, S. Filippone, N. Martin, and E. Palomares, Adv. Funct. Mater. **20**, 2695 (2010).

30) G. Garcia-Belmonte, P. P. Boix, J. Bisquert, M. Lenes, H. J. Bolink, A. La Rosa, S. Filippone, and N. Martin, J. Phys. Chem. Lett. **1**, 2566 (2010).

31) J. Zhao, Y. Li, G. Yang, K. Jiang, H. Lin, H. Abe, W. Ma, and H. Yan, Nature Energy **1**, 15027 (2016).

32) P. Hohenberg and W. Kohn, Phys. Rev. **136**, B864 (1964).

33) W. Kohn and L.J. Sham, Phys. Rev. **140**, A1133 (1965).

34) Y. Morikawa, K. Iwata, and K. Terakura, Appl. Surf. Sci. **169-170**, 11 (2001).

35) J.P. Perdew and Y. Wang, Phys. Rev. B **45**, 13244 (1992).

36) D.M. Ceperley and B.J. Alder, Phys. Rev. Lett. **45**, 566 (1980).

37) D. Vanderbilt, Phys. Rev. B **41**, 7892 (1990).

38) M. Maruyama and S. Okada, J. Phys. Soc. Jpn. **81**, 114719 (2012).

39) Y. Matsuo, A. Iwashita, Y. Abe, C. -Z. Li, K. Matsuo, M. Hashiguchi, and E. Nakamura, J. Am. Chem. Soc. **130**, 15429 (2008).

40) Y. Matsuo, Y. Sato, T. Niinomi, I. Soga, H. Tanaka, and E. Nakamura, J. Am. Chem. Soc. **131**, 16048 (2009).

41) Y. Matsuo, J. Kawai, H. Inada, T. Nakagawa, H. Ota, S Otsubo, and E.

Nakamura, Adv. Mater. **25**, 6266 (2013).
42) J. W. Ryan and Y. Matsuo, Sci. Rep. **5**, 8319 (2015).